
TEST-TIME MIXUP AUGMENTATION FOR DATA AND CLASS-DEPENDENT UNCERTAINTY ESTIMATION IN DEEP LEARNING IMAGE CLASSIFICATION

Hansang Lee & Haeil Lee

School of Electrical Engineering
Korea Advanced Institute of Science and Technology
Daehark 291, Yuseonggu, Daejeon 34141, Republic of Korea
{hansanglee, haeil.lee}@kaist.ac.kr

Helen Hong *

Department of Software Convergence
College of Interdisciplinary Studies for Emerging Industries
Seoul Women's University
Hwarangro 621, Nowongu, Seoul 01797, Republic of Korea
hlhong@swu.ac.kr

Junmo Kim

School of Electrical Engineering
Korea Advanced Institute of Science and Technology
Daehark 291, Yuseonggu, Daejeon 34141, Republic of Korea
junmo.kim@kaist.ac.kr

ABSTRACT

Uncertainty estimation of the trained deep learning networks is valuable for optimizing learning efficiency and evaluating the reliability of network predictions. In this paper, we propose a method for estimating uncertainty in deep learning image classification using test-time mixup augmentation (TTMA). To improve the ability to distinguish correct and incorrect predictions in existing aleatoric uncertainty, we introduce the TTMA data uncertainty (TTMA-DU) by applying mixup augmentation to test data and measuring the entropy of the predicted label histogram. In addition to TTMA-DU, we propose the TTMA class-dependent uncertainty (TTMA-CDU), which captures aleatoric uncertainty specific to individual classes and provides insight into class confusion and class similarity within the trained network. We validate our proposed methods on the ISIC-18 skin lesion diagnosis dataset and the CIFAR-100 real-world image classification dataset. Our experiments show that (1) TTMA-DU more effectively differentiates correct and incorrect predictions compared to existing uncertainty measures due to mixup perturbation, and (2) TTMA-CDU provides information on class confusion and class similarity for both datasets.

1 INTRODUCTION

Classification of medical images is a critical task for various applications, including disease diagnosis, surgical planning, and treatment prediction. Deep neural networks (DNNs) have achieved excellent accuracy on many image classification tasks and even outperformed human experts in some cases (Richens et al., 2020; De Fauw et al., 2018). However, DNNs can be difficult to interpret and lack a measure of reliability for their predictions, which can limit their use in real-world applications. To improve the trustworthiness of deep learning, researchers have focused on *uncertainty estimation*, which involves quantifying the confidence of a deep learning model in its decisions.

*Corresponding author

Several methods have been proposed to estimate the uncertainty for DNNs (Abdar et al., 2021). Kendall and Gal showed that the confidence of predictions for a Bayesian neural network directly represents the degree of uncertainty (Kendall & Gal, 2017). Gal and Ghahramani introduced the Monte-Carlo drop-out (MCDO) method, which estimates the model-based epistemic uncertainty by perturbing the network through drop-out and measuring the entropy of the prediction results (Gal & Ghahramani, 2016). Wang *et al.* proposed the test-time-augmentation (TTA) method to measure the data-based aleatoric uncertainty by perturbing the test data through affine transformation and measuring the entropy of the prediction results (Wang et al., 2019). Mukhoti *et al.* proposed using DNNs with inductive biases to capture both types of uncertainty by incorporating noise into the input features to model aleatoric uncertainty and utilizing Bayesian neural networks for modeling epistemic uncertainty (Mukhoti et al., 2021). Ghesu *et al.* proposed a system that learns not only the probabilistic estimate for classification but also an explicit uncertainty measure that captures the confidence of the system in the predicted output in order to enhance the performance and robustness of chest radiograph assessment (Ghesu et al., 2021).

In this paper, we propose a method for estimating the uncertainty of image classification with convolutional neural networks (CNNs) using test-time mixup augmentation (TTMA). The method is based on the idea that mixup augmentation on training data plays a crucial role in regularizing the learner by emphasizing the boundary regions between different classes in the latent feature space Zhang et al. (2018). Our proposed method involves two different uncertainty measures calculated using the TTMA approach: the TTMA data uncertainty and the TTMA class-dependent uncertainty. The first *TTMA data uncertainty (TTMA-DU)* is computed by applying mixup to test data with partners uniformly sampled from all training classes and measuring the entropy of the predictions made on the mixup data. From an aleatoric uncertainty perspective, the proposed TTMA-DU is able to more accurately distinguish correct predictions from incorrect predictions than existing TTA and MCDO methods thanks to the more aggressive perturbation property of mixup augmentation. The second *TTMA class-dependent uncertainty (TTMA-CDU)* is computed by applying mixup to test data with partners sampled from a specific training class and measuring the entropy of the predictions made on the mixup data. The proposed TTMA-CDU is distinct from existing aleatoric uncertainty measures in that it is defined by both test data and the trained class. We hypothesize that this measure provides insight into the class confusion and similarity of the trained network, and confirm it through experiments. To validate the effectiveness of our proposed method, we conduct experiments on two image classification datasets with different characteristics: the ISIC-18 skin lesion dataset, which is similar to other common medical imaging datasets, and the CIFAR-100 natural image dataset, which is similar to other common natural image datasets. The results of our experiments show that the proposed method yields consistent results on both datasets, regardless of their different characteristics.

The main contributions of this work are as follows.

- We propose a *TTMA data uncertainty (TTMA-DU)*, an aleatoric uncertainty measure that outperforms existing TTA uncertainty in evaluating the reliability of network predictions.
- We propose a *TTMA class-dependent uncertainty (TTMA-CDU)*, a first aleatoric uncertainty measure associated with a specific class, which provides insight into class confusion and similarity within the trained network.
- The effectiveness of these uncertainty measures is demonstrated through experiments on two public image classification datasets of varying characteristics.

The remainder of this paper is organized as follows. In Section 2, we summarize the theoretical background on uncertainty estimation and mixup augmentation. The details of our proposed method are presented in Section 3, with the experimental materials, results and evaluations provided in Section 4. The discussions and analyses of the proposed method and contributions are reported in Section 5, and the paper concludes with future research directions in Section 6.

2 RELATED WORKS

2.1 UNCERTAINTY ESTIMATION

Uncertainty estimation is the task of measuring the degree of confidence of a deep learning model regarding its decisions (Gawlikowski et al., 2021). This can be important for various applications, as

it allows a model to provide a measure of its own confidence in its predictions, which can be useful for decision-making purposes (Abdar et al., 2021). There are two types of uncertainty: *aleatoric uncertainty*, which is the inherent noise or randomness in the data, and *epistemic uncertainty*, which is the uncertainty due to the model not being aware of the true underlying probability distribution. Uncertainty estimation can be accomplished by measuring various statistical properties, such as entropy or variance, of the predicted probability distribution. Uncertainty estimation is useful in a variety of applications, such as improving the learning efficiency (Gal et al., 2017; Zhao et al., 2021; Hong et al., 2020; Rizve et al., 2021; Nielsen & Okoniewski, 2019), evaluating the reliability of the network prediction, data-efficiency, decision making, and safety-critical applications such as medical diagnosis (Martin et al., 2019; Ayhan et al., 2020; Cicalese et al., 2021; Carneiro et al., 2020; Singh et al., 2020; Herzog et al., 2020; Shamsi et al., 2021; Wang et al., 2021; Czolbe et al., 2021; Matsunaga et al., 2017; Graham et al., 2019) or self-driving cars (Hoel et al., 2020b;a; Tang et al., 2022).

There are several approaches to uncertainty estimation for deep learning, including ensembles, Bayesian neural networks, dropout, and Monte Carlo sampling. Ensemble methods involve training multiple models on the same data and combining their predictions to obtain a more accurate and uncertain estimate (Lakshminarayanan et al., 2017). Bayesian neural networks incorporate a Bayesian framework into the training process to explicitly model the uncertainty in the model’s parameters (Blundell et al., 2015). Dropout involves randomly setting the output of specific neurons to zero during training to introduce the epistemic uncertainty into the model (Gal & Ghahramani, 2016). Monte Carlo sampling involves sampling multiple sets of model parameters and averaging the predictions to obtain an uncertainty estimate Kendall & Gal (2017).

Test-time augmentation (TTA) is a technique used to improve the performance of machine learning models by augmenting the test data with various transformations of the original data (Matsunaga et al., 2017). These transformations can include image rotation, scaling, flipping, and cropping. In the context of uncertainty estimation, the TTA involves estimating the uncertainty of the model’s predictions based on the augmented test data Wang et al. (2019). Due to its simple implementation and efficiency, the TTA uncertainty estimation has been widely used for various applications in medical image analysis (Wang et al., 2019; Graham et al., 2019).

2.2 MIXUP AUGMENTATION

Mixup is a recently proposed data augmentation technique that creates synthetic training examples by interpolating between pairs of examples and their labels using a convex combination. The weight of each example is determined by a mixing coefficient α which is drawn from a beta distribution. This technique, which was first introduced by Zhang *et al.*, is considered a variation of consistency regularization methods, specifically mixed sample data augmentation (Zhang et al., 2018). Mixup has been shown to improve the generalization performance of deep neural networks on a variety of tasks, including image recognition (Yun et al., 2019; Qin et al., 2020; Kim et al., 2020a; Uddin et al., 2021; Dabouei et al., 2021), semantic segmentation (French et al., 2019; Ghiasi et al., 2021; Su et al., 2021; Kim et al., 2020b; Zhou et al., 2022), natural language processing (Guo et al., 2019; Sun et al., 2020; Bari et al., 2020; Si et al., 2020; Chen et al., 2020), video processing (Yun et al., 2020; Li et al., 2021; Kim et al., 2020c; Kahatapitiya et al., 2021), and medical image analysis (Eaton-Rosen et al., 2018; Chaitanya et al., 2020; Zhao et al., 2019; Panfilov et al., 2019; Li et al., 2019; Verma et al., 2019; Jung et al., 2019). The simplicity and effectiveness of Mixup make it a valuable tool for deep learning practitioners to consider when working on a wide range of applications.

Since the original proposal of mixup, there have been several related works that have extended the idea in various ways. Verma *et al.* suggested a variant of mixup called Manifold Mixup, which uses geodesic interpolation on the hidden representations of the data instead of interpolating between the data and its labels (Verma et al., 2019). Yun *et al.* proposed CutMix, which creates synthetic training examples by combining sub-regions of multiple images and their labels (Yun et al., 2019). CutMix has been shown to be particularly effective for object detection tasks, where it can improve the localization performance of the model. Kim *et al.* suggested PuzzleMix, which creates synthetic training examples by jigsaw shuffling and linearly interpolating between pairs of images (Kim et al., 2020a). Hendrycks *et al.* proposed AugMix which creates synthetic training examples by applying a series of random image transformations to a single image, rather than interpolating between multiple images as in mixup (Hendrycks* et al., 2020). AugMix has been shown to improve the robustness of models

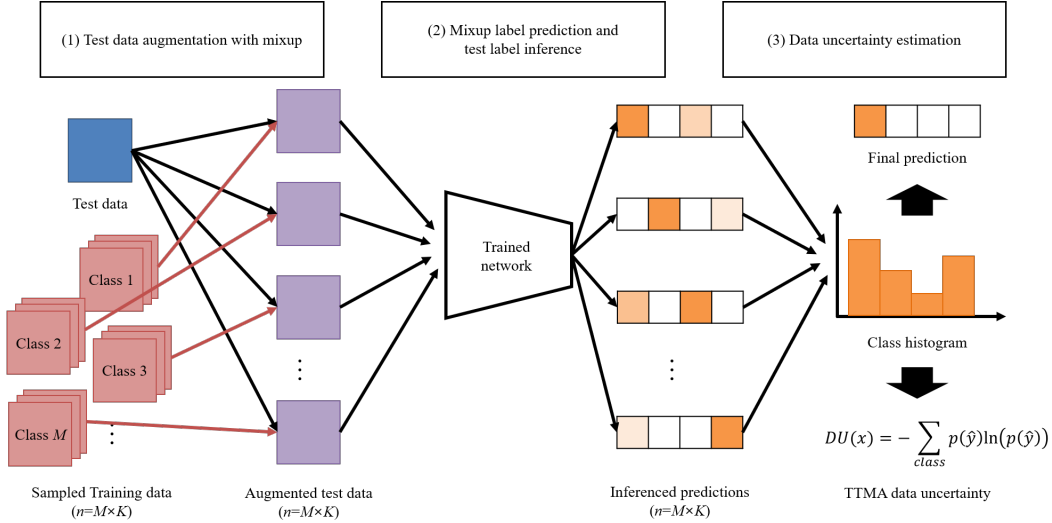


Figure 1: A pipeline of the proposed TTMA data uncertainty (TTMA-DU) estimation method.

to various types of image perturbations, such as noise, blur, and color distortion. Liu *et al.* suggested AutoMix that uses reinforcement learning to learn an optimal mixing strategy, by searching over different data augmentation techniques and interpolation coefficients (Liu et al., 2021).

Various attempts have also been made to explain the effect and behavior of mixup. Thulasidasan *et al.* found that mixup training can improve the calibration of deep neural networks, which means that the predicted probabilities of the model are more closely aligned with the true underlying probabilities of the data (Thulasidasan et al., 2019). Zhang *et al.* further showed that the effect of the mixup on calibration is highly dependent on the specific characteristics of the data and the model (Zhang et al., 2021). Wen *et al.* observed that combining ensembles and data augmentation can lead to significant degradation in the calibration of machine learning models (Wen et al., 2021). They also provided a theoretical analysis of the reasons for this effect and suggested that it may be due to the increased complexity of the model and the increased variance in the predictions. Zhang *et al.* also provided the theoretical analysis on how the mixup improves generalization and robustness to the adversarial attacks by proving that the mixup is approximately a regularized loss minimization.

3 METHODS

3.1 TTMA DATA UNCERTAINTY

The proposed *TTMA data uncertainty (TTMA-DU)* aims to enhance TTA uncertainty by replacing the affine augmentation with mixup augmentation for test data. The proposed method consists of three steps: (1) test data augmentation with mixup, (2) mixup label prediction and test label inference, and (3) TTMA-DU estimation. The pipeline of the proposed TTMA-DU estimation method is summarized in Fig. 1.

3.1.1 TEST DATA AUGMENTATION WITH MIXUP

First, we apply mixup augmentation to the test data to obtain perturbation-robust results and to estimate the uncertainty. Let us have a training image-label pair $(x_{train}, y_{train}) \in S_{train}$, test image-label pair $(x_{test}, y_{test}) \in S_{test}$, where $x \in \mathbb{R}^{W \times H}$ is an input image with width of W and height of H , and $y \in \mathbb{R}^M$ is a soft label vector with a size of M classes. For a given test data (x_{test}, y_{test}) , we form a mixup test data (x_{mixup}, y_{mixup}) by combining the test data with randomly sampled training data (x_{train}, y_{train}) as follows.

$$x_{mixup}(m, k) = \lambda x_{test} + (1 - \lambda)x_{train}(m, k) \quad (1)$$

$$y_{mixup}(m, k) = \lambda y_{test} + (1 - \lambda) y_{train}(m, k) \quad (2)$$

where $(x_{train}(m, k), y_{train}(m, k))$ is a training image-label pair of k -th data randomly sampled from class $m \in \{1, \dots, M\}$, and λ is a mixup coefficient determined by the beta distribution variable $\lambda \sim \mathcal{B}(\alpha, \alpha)$. This process generates a total of $M \times K$ mixup-augmented data for one test data, where K is a number of sampled training data.

3.1.2 MIXUP LABEL PREDICTION AND TEST LABEL INFERENCE

In this step, the mixup-trained network $f : \mathbb{R}^{W \times H} \rightarrow \mathbb{R}^M$, which is trained on a training set S_{train} , is used to predict the soft label of the mixup-augmented test data $\hat{y}_{mixup}(m, k) = f(x_{mixup}(m, k))$. The label of the test data $\hat{y}_{test}(m, k)$ is then inferred from this prediction result. From Eq. 2, we have

$$y_{test} = (y_{mixup}(m, k) - (1 - \lambda) y_{train}(m, k)) / \lambda \quad (3)$$

By replacing the true labels $y_{test}, y_{mixup}(m, k)$ with the inferred label of the test data $\hat{y}_{test}(m, k)$ and the predicted label of the mixup-augmented data $\hat{y}_{mixup}(m, k) = f(x_{mixup}(m, k))$, respectively, we can rewrite Eq. 3 as

$$\hat{y}_{test}(m, k) = (f(x_{mixup}(m, k)) - (1 - \lambda) y_{train}(m, k)) / \lambda \quad (4)$$

From Eq. 4, we can obtain a total of $M \times K$ inferred labels for one test data.

3.1.3 TTMA DATA UNCERTAINTY ESTIMATION

From a total of $M \times K$ inferred soft labels for the test data $\hat{y}_{test}(m, k)$, we can have a histogram of hard labels $\hat{\mathcal{Y}}_{test} = \{\arg \max_l \hat{y}_{test}(m, k), m = 1, \dots, M, k = 1, \dots, K\}$ where $l = 1, \dots, M$ is a class index for hard label. From the histogram of inferred hard labels $\hat{\mathcal{Y}}_{test}$, the final test label \hat{y}_{test} can be obtained using majority voting by

$$\hat{y}_{test} = \arg \max_l P_l(\hat{\mathcal{Y}}_{test}) \quad (5)$$

where $P_l(\hat{\mathcal{Y}}_{test})$ is a probability that the histogram of $\hat{\mathcal{Y}}_{test}$ has a class $l = 1, \dots, M$.

The TTMA-DU is then computed as the entropy of the histogram of inferred labels $\hat{\mathcal{Y}}_{test}$ by

$$DU(x_{test}) = - \sum_{l=1}^M P_l(\hat{\mathcal{Y}}_{test}) \ln(P_l(\hat{\mathcal{Y}}_{test})). \quad (6)$$

The proposed TTMA-DU illustrates the instability of test data predictions caused by mixing various classes. It uses more intense perturbations than traditional affine-based transformations, allowing for an evaluation of the trained network's robustness to data-based perturbations in harsher conditions than those provided by existing TTA method (Wang et al., 2019).

3.2 TTMA CLASS-DEPENDENT UNCERTAINTY

In the computation of TTMA-DU, a mixup is performed with the same number of sampled data from all classes to apply unbiased perturbation to the test data. However, this raises the question of how the uncertainty measures appear and which information they can provide when they are based on the test data perturbed only by a mixup with the training data of a specific class. We refer to this as *TTMA class-dependent uncertainty (TTMA-CDU)*. To address this, the proposed method for estimating TTMA-CDU involves three steps: (1) Test data augmentation with mixup, (2) mixup label prediction and test label inference, and (3) TTMA-CDU estimation. The pipeline of the proposed TTMA-CDU estimation method is summarized in Fig. 2.

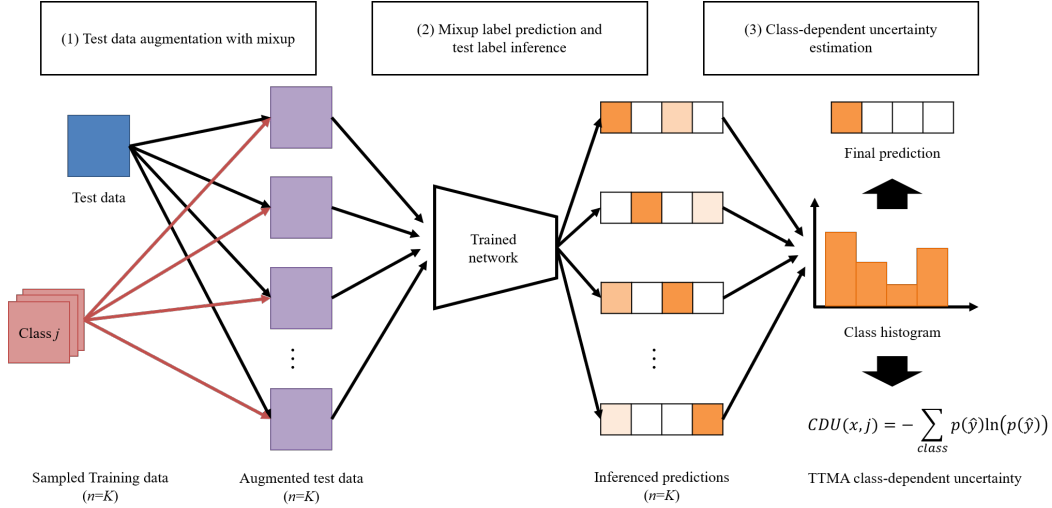


Figure 2: A pipeline of the TTMA class-dependent (TTMA-CDU) uncertainty estimation method.

3.2.1 TEST DATA AUGMENTATION WITH MIXUP

First, we apply mixup augmentation to the test data with the training data sampled from a specific class $j \in \{1, \dots, M\}$ to obtain perturbation-robust results and to estimate the uncertainty. Let us have a training image-label pair $(x_{train}, y_{train}) \in S_{train}$, test image-label pair $(x_{test}, y_{test}) \in S_{test}$, where $x \in \mathbb{R}^{W \times H}$ is an input image with width of W and height of H , and $y \in \mathbb{R}^M$ is a soft label vector with a size of M classes. For a given test data (x_{test}, y_{test}) , we form a mixup test data (x_{mixup}, y_{mixup}) by combining the test data with randomly sampled training data (x_{train}, y_{train}) as follows.

$$x_{mixup}(j, k) = \lambda x_{test} + (1 - \lambda)x_{train}(j, k) \quad (7)$$

$$y_{mixup}(j, k) = \lambda y_{test} + (1 - \lambda)y_{train}(j, k) \quad (8)$$

where $(x_{train}(j, k), y_{train}(j, k))$ is a training image-label pair of k -th data randomly sampled from training set of class j , and λ is a mixup coefficient determined by the beta distribution variable $\lambda \sim \mathcal{B}(\alpha, \alpha)$. This process generates a total of K mixup-augmented data for one test data, where K is a number of sampled training data.

3.2.2 MIXUP LABEL PREDICTION AND TEST LABEL INFERENCE

The mixup-trained network $f : \mathbb{R}^{W \times H} \rightarrow \mathbb{R}^M$, which is trained on a training set S_{train} , is used to predict the soft label of the mixup-augmented test data $\hat{y}_{mixup}(j, k) = f(x_{mixup}(j, k))$. The label of the test data $\hat{y}_{test}(j, k)$ is then inferred from this prediction result. From Eq. 8, we have

$$y_{test} = (y_{mixup}(j, k) - (1 - \lambda)y_{train}(j, k)) / \lambda \quad (9)$$

By replacing the true labels $y_{test}, y_{mixup}(j, k)$ with the inferred label of the test data $\hat{y}_{test}(j, k)$ and the predicted label of the mixup-augmented data $\hat{y}_{mixup}(j, k) = f(x_{mixup}(j, k))$, respectively, we can rewrite Eq. 9 as

$$\hat{y}_{test}(j, k) = (f(x_{mixup}(j, k)) - (1 - \lambda)y_{train}(j, k)) / \lambda \quad (10)$$

From Eq. 10, we obtain a total of K inferred labels for one test data.

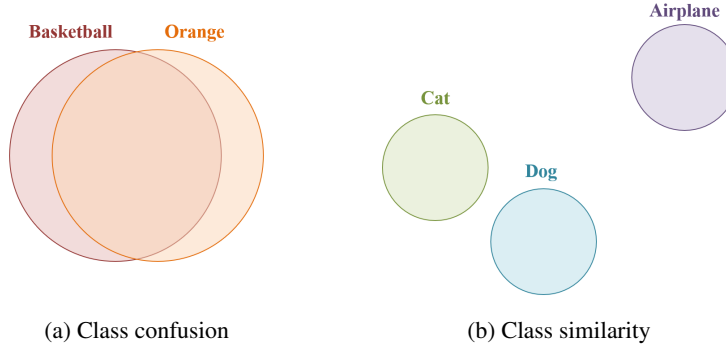


Figure 3: Diagrams of feature space overview for (a) class confusion and (b) class similarity.

3.2.3 TTMA CLASS-DEPENDENT UNCERTAINTY ESTIMATION

From a total of K inferred soft labels for the test data $\hat{y}_{test}(j, k)$, we can have a histogram of hard labels $\hat{\mathcal{Y}}_{test,j} = \{\arg \max_l \hat{y}_{test}(j, k), k = 1, \dots, K\}$ where $l = 1, \dots, M$ is a class index for hard label. From the histogram of inferred hard labels $\hat{\mathcal{Y}}_{test,j}$, the final test label $\hat{y}_{test,j}$ can be obtained using majority voting by

$$\hat{y}_{test,j} = \arg \max_l P_l \left(\hat{\mathcal{Y}}_{test,j} \right) \quad (11)$$

where $P_l(\hat{\mathcal{Y}}_{test,j})$ is a probability that the histogram of $\hat{\mathcal{Y}}_{test,j}$ has a class $l = 1, \dots, M$.

The TTMA-CDU is then computed as the entropy of the histogram of inferred labels $\hat{\mathcal{Y}}_{test,j}$ by

$$CDU(x_{test}, j) = - \sum_{l=1}^M P_l \left(\hat{\mathcal{Y}}_{test,j} \right) \ln \left(P_l \left(\hat{\mathcal{Y}}_{test,j} \right) \right). \quad (12)$$

The TTMA-CDU represents the instability of predictions of the test data due to perturbations from the mixup with a specific class.

3.2.4 INTERPRETATION OF TTMA CLASS-DEPENDENT UNCERTAINTY

The proposed TTMA-CDU is a novel uncertainty measure that takes test data and a class as variables. Its unique capability is to provide information about the relationship between test data and a specific class. Two types of information that it can provide are *class confusion* and *class similarity*. To understand class confusion and class similarity, we introduce the average feature distance (AFD) between the test data x_{test} and the specific class j , which can be calculated as

$$AFD(x_{test}, j) = \frac{1}{K} \sum_{k=1}^K d(v_{test}, v_{train}(j, k)), \quad (13)$$

where K is a number of sampled training data in class j , $v_{test}, v_{train}(j, k)$ are feature vectors obtained from the input data $x_{test}, x_{train}(j, k)$ in the network, respectively, and $d(u, v) = 1 - (u \cdot v) / (\|u\| \|v\|)$ is a cosine distance between u and v . We demonstrate how AFD and CDU represent class confusion and similarity by comparing two measures in two circumstances shown in Fig. 3.

Class confusion occurs when the network struggles to distinguish between two classes, such as mistaking a basketball for an orange. As shown in Fig. 3 (a), in the feature space, it is characterized by overlap in the distributions of the two classes, leading to low AFD. The TTMA-CDU, however, will have high values in cases of class confusion due to evenly distributed predictions of mixup data.

Class similarity, on the other hand, refers to when the network recognizes two classes as similar, but can clearly distinguish them. For example, a dog and a cat would have higher class similarity than a dog and an airplane, as they belong to the same category. In the feature space, as shown in Fig. 3 (b), class similarity can be defined as the negative of the AFD between the two class distributions. The TTMA-CDU will have lower values for class similarity, as mixup with a similar class will increase prediction instability less than with a dissimilar class.

In analyzing the performance and behavior of a prediction network, it is crucial to differentiate between class confusion and class similarity. The traditional method of using AFD alone is not sufficient, as it has low values for both types of class relationship. The combination of AFD and TTMA-CDU allows for discrimination between the two.

4 EXPERIMENTS

4.1 DATASETS AND IMPLEMENTATION

The proposed method was tested using two public datasets, ISIC-18 and CIFAR-100. ISIC-18 (Codella et al., 2017; 2018; 2019) is a medical image dataset that contains 10,208 images of skin lesions for 7 different skin diseases (Tschandl et al., 2018; Combalia et al., 2019). The dataset is split into 10,015 images for training and 193 images for validation. Fig. 4 shows examples of images for each disease in the dataset, and Table 1 summarizes the statistics of the data for each disease. However, the small size of the dataset and the class imbalance present a risk of overfitting (Zhang et al., 2019). Additionally, the dataset contains examples of both inter-class similarity and intra-class variation, which makes it challenging for accurate classification.

A VGG-19 model (Simonyan & Zisserman, 2015) was trained on the ISIC-18 dataset for 300 epochs using a mini-batch size of 128. The initial learning rate was set to 0.01 and was decreased by 10 after 150 and 225 epochs. To improve the performance of the model, both affine and mixup data augmentation were applied during the training process. Additionally, drop-out was applied on fully connected layers. The affine data augmentation included a random horizontal flip, a random vertical flip, a random rotation between -45 and 45 degrees, a random translation with shift rates of (0.1,0.1), and a random scaling with a factor of 1 to 1.2. In mixup augmentation, the mixup hyper-parameter α was set to 0.2. The drop-out probability for fully connected layers was set to 0.5.

During the testing phase, augmentation methods suitable for each case, TTA, MCDO, and TTMA, were applied to the test data using the same parameters used during the training process. For TTA, affine augmentation was applied to the test data. For MCDO, drop-out was applied to the trained network on fully connected layers with a drop-out probability of 0.5. For TTMA, mixup augmentation with $\alpha = 0.2$ was applied to the test data, where the number of selected training data for each class to compute the mixup was set to $K = 30$. This resulted in $MK = 210$ mixup augmented test data per one original test data.

A Wide Residual Network (WRN-28-10) model (Zagoruyko & Komodakis, 2016) was trained on the CIFAR-100 dataset for 200 epochs using a mini-batch size of 256. The initial learning rate

Table 1: Statistics on the amount of data by disease class for the training and validation sets in the ISIC-18 dataset. (AKIEC: Actinic keratosis, BCC: Basal cell carcinoma, BKL: Benign keratosis, DF: Dermatofibroma, MEL: Melanoma, NV: Melanocytic nevus, VASC: Vascular lesion)

Classes	Training	Validation
AKIEC	327	8
BCC	514	15
BKL	1099	22
DF	115	1
MEL	1113	21
NV	6705	123
VASC	142	3
Total	10015	193

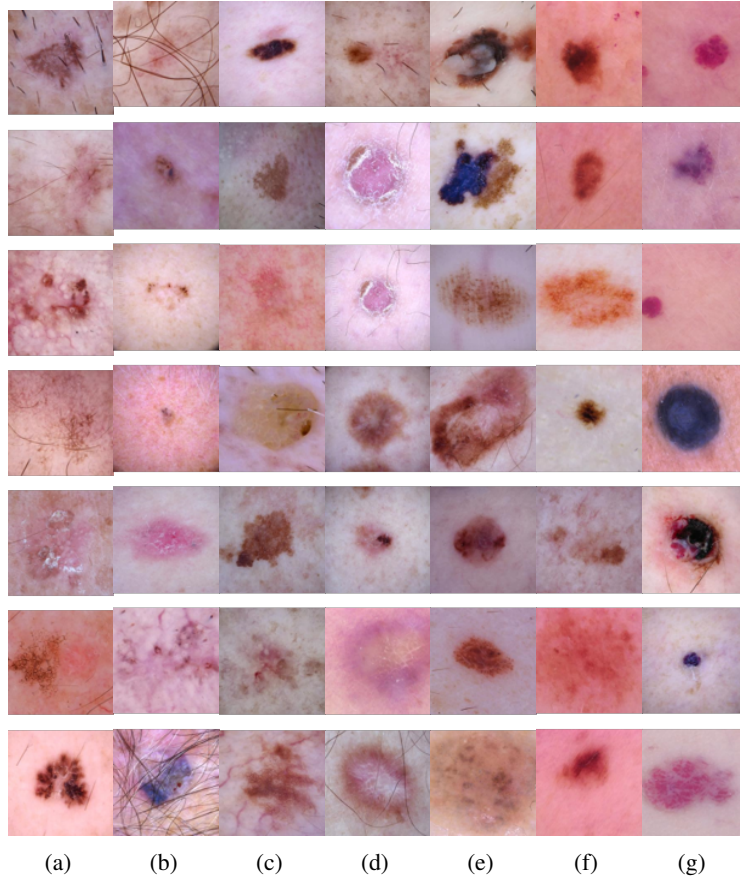


Figure 4: Examples of ISIC-18 skin lesion images for different disease classes: (a) AKIEC, (b) BCC, (c) BKL, (d) DF, (e) MEL, (f) NV, (g) VASC.

was set to 0.1 and was decreased by 5 after 60, 120, and 160 epochs. To improve the performance of the model, both affine and mixup data augmentation were applied during the training process. Additionally, drop-out was applied on fully connected layers. The affine data augmentation included random cropping with a square size of 32, a random horizontal flip, a random rotation between -45 and 45 degrees, a random translation with shift rates of $(0.1, 0.1)$, and a random scaling with a factor of 1 to 1.2. In mixup augmentation, the mixup hyper-parameter α was set to 0.2. The drop-out probability for fully connected layers was set to 0.3.

During the testing phase, augmentation methods suitable for each case, TTA, MCDO, and TTMA, were applied to the test data using the same parameters used during the training process. For TTA, affine augmentation was applied to the test data. For MCDO, drop-out was applied to the trained network on fully connected layers with a drop-out probability of 0.3. For TTMA, mixup augmentation with $\alpha = 0.2$ was applied to the test data, where the number of selected training data for each class to compute the mixup was set to $K = 10$. This resulted in $MK = 1,000$ mixup augmented test data per original test data. These experiments were run on eight NVIDIA RTX 2080 Ti GPU machines using PyTorch.

4.2 EVALUATION AND COMPARISON

We compared the proposed methods with different types of uncertainty estimation methods to validate their effectiveness. Specifically, we compared the proposed TTMA-DU with (1) the aleatoric uncertainty measured by the conventional TTA method (Wang et al., 2019), and (2) the epistemic uncertainty measured by the conventional MCDO method (Gal & Ghahramani, 2016). We also analyzed the sensitivity of the internal parameters α and K of the proposed TTMA-DU, where

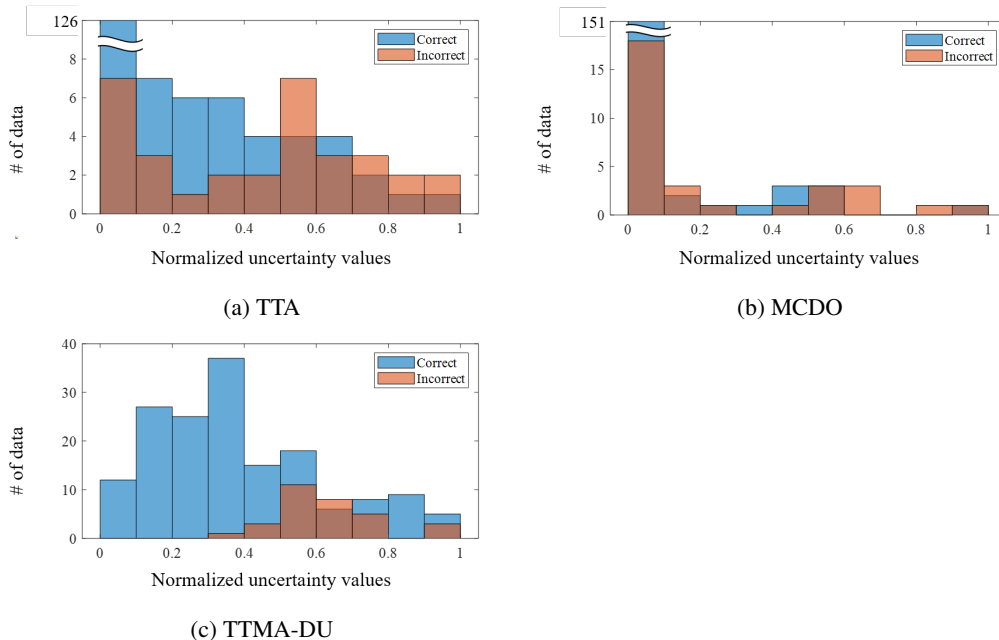


Figure 5: Histograms of aleatoric uncertainty for correct and incorrect test samples for ISIC-18 classification results with (a) TTA, (b) MCDO, and (c) TTMA-DU methods. In (a) TTA, the number of correct samples having uncertainty of $[0,0.1)$ is 126. In (b) MCDO, the number of correct samples having uncertainty of $[0,0.1)$ is 151.

α is the mixup weight hyper-parameter and K is the number of selected training data per class for the mixup. We performed these comparisons using the ISIC-18-trained VGG-19 model with $\alpha \in \{0, 0.2, 0.4, 0.6, 0.8, 1\}$ and $K \in \{10, 20, 30, 40, 50\}$, and the CIFAR-100-trained WRN-28-10 model with $\alpha \in \{0, 0.2, 0.4, 0.6, 0.8, 1\}$ and $K \in \{5, 10, 15, 20\}$.

To determine if the proposed TTMA-DU method is better at distinguishing correct predictions from incorrect predictions than the conventional aleatoric uncertainty method, we analyzed the uncertainty histograms of correct and incorrect test samples and the accuracy-rejection curves. The histograms allow us to compare the distributions of uncertainty for correct and incorrect predictions. A smaller overlap between the two distributions indicates better discrimination. The accuracy-rejection curves show the relationship between rejection rate and accuracy by rejecting test data with the top T uncertainty level, where T ranges from 0 to 95%. The more the curve monotonically increases and the steeper the slope, the better the uncertainty method discriminates correct predictions from incorrect predictions.

To determine if the proposed TTMA-CDU method provides information about class confusion and similarity, we compared the TTMA-CDU for each class to the Average Feature Distance (AFD) in feature space. The AFD is computed as the average of the cosine feature distances between a test data point and the training data belonging to the same class. We used boxplots of the TTMA-CDU and AFD with feature distributions visualized through t-SNE (van der Maaten & Hinton, 2008) to verify if the proposed TTMA-CDU can help distinguish class confusion and similarity.

4.3 RESULTS: SKIN LESION DIAGNOSIS ON ISIC-18

4.3.1 TTMA DATA UNCERTAINTY ON ISIC-18

Fig. 5 presents histograms of the aleatoric uncertainty for correct and incorrect test data for TTA, MCDO, and the proposed TTMA-DU. The ideal histogram would show clear distinction between the two distributions, with correct samples concentrated in the low uncertainty area and incorrect samples concentrated in the high uncertainty area. However, TTA and MCDO have considerable overlap in their uncertainty distributions of correct and incorrect test samples, making it challenging

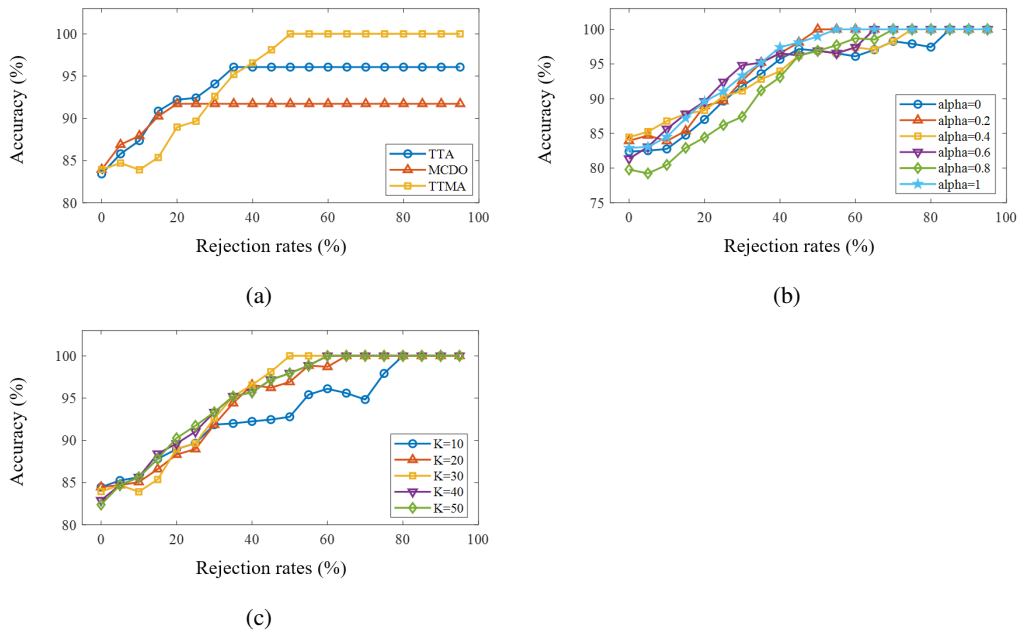


Figure 6: Accuracy-rejection curves of ISIC-18 skin lesion classification results with (a) different uncertainty estimation methods, (b) different values of mixup hyper-parameter α , and (c) different values of mixup sampling number K for TTMA-DU.

to differentiate between them. In contrast, the proposed TTMA-DU method shows distributions that are more distinguishable. Additionally, with the TTMA-DU, we can achieve 100% accurate predictions by thresholding the normalized uncertainty at a value of less than 0.3.

Fig.6 displays the accuracy-rejection curves for different uncertainty estimation methods, different values of α , and different values of K using the proposed TTMA-DU. Table2 summarizes the rejection accuracy for the proposed and comparative methods. In Fig. 6 (a), TTA reaches a maximum of 96.1% accuracy at 35% rejection, while MCDO reaches a maximum of 91.7% accuracy with 20% rejection. Starting with an accuracy of 83.9% at 0% rejection, the proposed TTMA has a monotonically increasing curve, reaching 100% accuracy at 50% rejection. In Fig.6 (b), it can be seen that the TTMA with a mixup weight parameter of $\alpha = 0.2$ reaches 100% accuracy most rapidly at 50% rejection, compared to the other values of α . Similarly, in Fig.6 (c), it can be observed that the TTMA with $K = 30$ reaches 100% accuracy most rapidly at 50% rejection, compared to the other

Table 2: Performance evaluation and comparisons of ISIC-18 skin lesion classification with different uncertainty estimation methods. Accuracy (%) was evaluated on the rejected test data for various rejection rates $T \in \{0\%, 25\%, 50\%, 75\%, 95\%\}$.

Methods	Rejection rates				
	0	25	50	75	95
Single	83.4				
TTA	83.4	92.4	96.1	96.1	96.1
MCDO	83.9	91.7	91.7	91.7	91.7
TTMA-DU ($\alpha = 0.0$)	82.4	89.7	96.9	97.9	100
TTMA-DU ($\alpha = 0.2$)	83.9	89.7	100	100	100
TTMA-DU ($\alpha = 0.4$)	84.5	90.3	96.9	100	100
TTMA-DU ($\alpha = 0.6$)	81.3	92.4	96.9	100	100
TTMA-DU ($\alpha = 0.8$)	79.8	86.2	96.9	100	100
TTMA-DU ($\alpha = 1.0$)	82.9	91.0	99.0	100	100

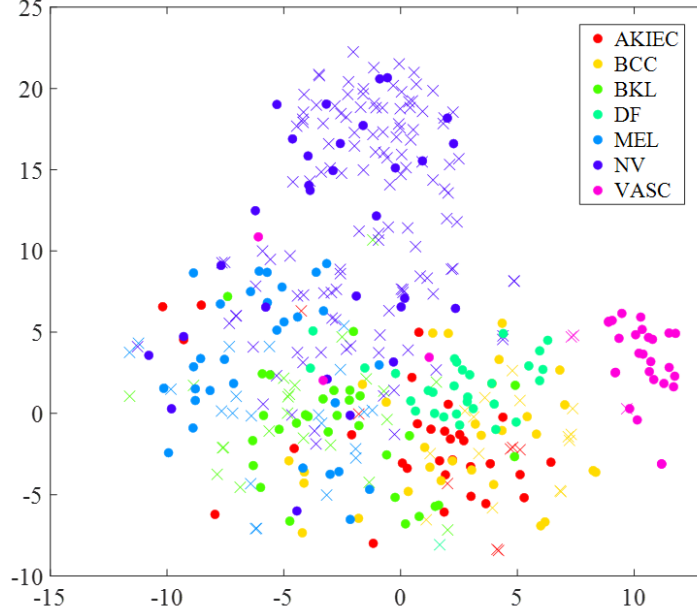


Figure 7: tSNE feature distributions of training (marked as o) and validation (marked as x) data in the ISIC-18 skin lesion classification results.

values of K . It can be confirmed that the proposed TTMA-DU demonstrates better performance in distinguishing correct predictions from incorrect predictions compared to existing TTA and MCDO methods.

4.3.2 TTMA CLASS-DEPENDENT UNCERTAINTY ON ISIC-18

Fig. 7 illustrates the t-SNE feature distributions of the sampled training and validation data of the ISIC-18 dataset. The feature distributions of four classes, AKIEC, BCC, BKL, and DF, largely overlap in the lower center, while MEL, NV, and VASC appear densely distributed in different corners. As a result, it can be expected that the four overlapping classes will have high TTMA-CDU and low AFD values, and that the remaining three classes will have TTMA-CDU distributions that are similar to those of the AFD.

Figs. 8 and 9 illustrate boxplots of TTMA-CDU and AFD for the AKIEC and MEL classes, respectively. In Fig. 8, the classes that overlap with AKIEC in tSNE feature space, i.e. BCC, BKL, and DF, have lower AFD compared to the distant classes, i.e. MEL, NV, and VASC, but higher TTMA-CDU. In Fig. 9, however, the TTMA-CDU for MEL class which has no overlap with other classes in feature space is entirely similar to its AFD. This confirms that the TTMA-CDU not only provides information about class similarity like AFD but also can distinguish class confusion from class similarity through its combination with AFD.

4.4 RESULTS: NATURAL IMAGE CLASSIFICATION ON CIFAR-100

4.4.1 TTMA DATA UNCERTAINTY ON CIFAR-100

Fig. 10 illustrates histograms of the aleatoric uncertainty for correct and incorrect test data for TTA, MCDO, and the proposed TTMA-DU. For TTA and MCDO, many correct samples are distributed in the lowest uncertainty region at $[0,0.05)$, and also in the higher uncertainty region, making it difficult to differentiate between correct and incorrect samples. In contrast, the proposed TTMA-DU shows almost no incorrect samples in the lowest uncertainty region at $[0,0.05)$ and a shift of the overall distribution to the higher uncertainty region, making it relatively more distinguishable compared to

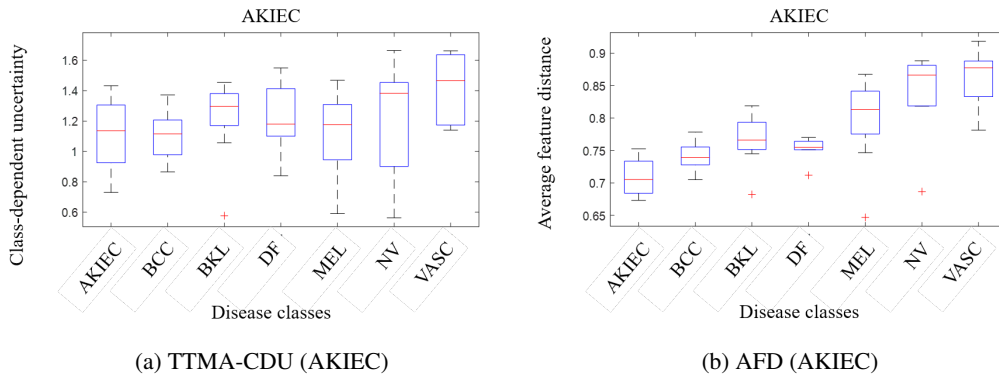


Figure 8: Boxplots of (a) TTMA class-dependent uncertainty (TTMA-CDU) and (b) average feature distance (AFD) for actinic keratosis (AKIEC) class in the ISIC-18 classification results.

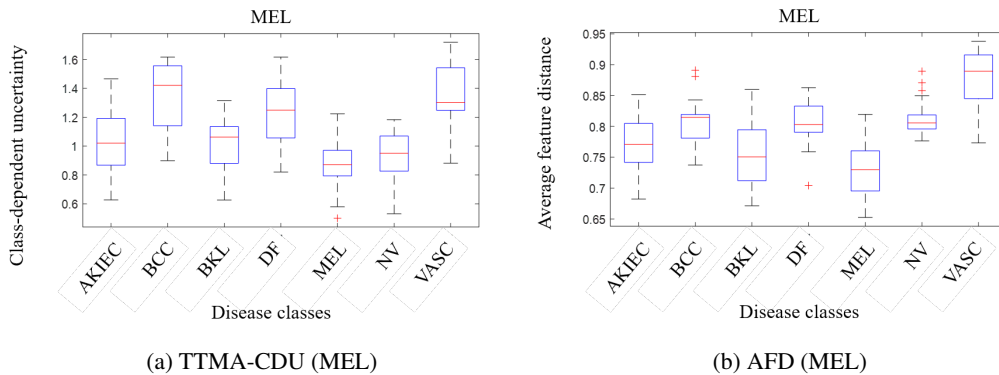


Figure 9: Boxplots of (a) TTMA class-dependent uncertainty (TTMA-CDU) and (b) average feature distance (AFD) for melanoma (MEL) class in the ISIC-18 classification results.

other methods. Additionally, using the TTMA-DU with a threshold of less than 0.2, 100% accurate predictions can be obtained through uncertainty thresholding.

Fig. 11 illustrates the accuracy-rejection curves for (a) different uncertainty estimation methods, and with (b) different values of α , and (c) different values of K with the proposed TTMA-DU method. Table 3 summarizes the rejection accuracy for the proposed and comparative methods. In Fig. 11 (a), TTA shows a curve that increases steeply from a low 0% rejection accuracy, whereas MCDO shows a curve that is saturated at 50% rejection accuracy. In contrast, the proposed TTMA-DU method starts with a similar 0% rejection accuracy to MCDO, but shows a curve that increases monotonically as the rejection rate increases, achieving the highest 95% rejection accuracy. In Fig. 11 (b), it can be observed that TTMA-DU with a mixup weight parameter $\alpha = 0.2$ achieves the highest 95% rejection accuracy compared to other choices of α . Fig. 11 (c) indicates that the accuracy-rejection characteristics of the proposed TTMA-DU are relatively less affected by the number of mixup samples K . Similar to the ISIC results, the proposed TTMA-DU shows improved performance in distinguishing correct predictions from incorrect predictions in natural image classification, compared to TTA and MCDO.

4.4.2 TTMA CLASS-DEPENDENT UNCERTAINTY ON CIFAR-100

Fig. 12 illustrates tSNE feature distributions of the sampled training and validation data in CIFAR-100. Unlike ISIC-18, the feature distribution of CIFAR-100 has almost no overlap between the classes, and the data of each class are densely distributed. This implies that it can be expected that the TTMA-CDU will provide only information about class similarity, rather than class confusion.

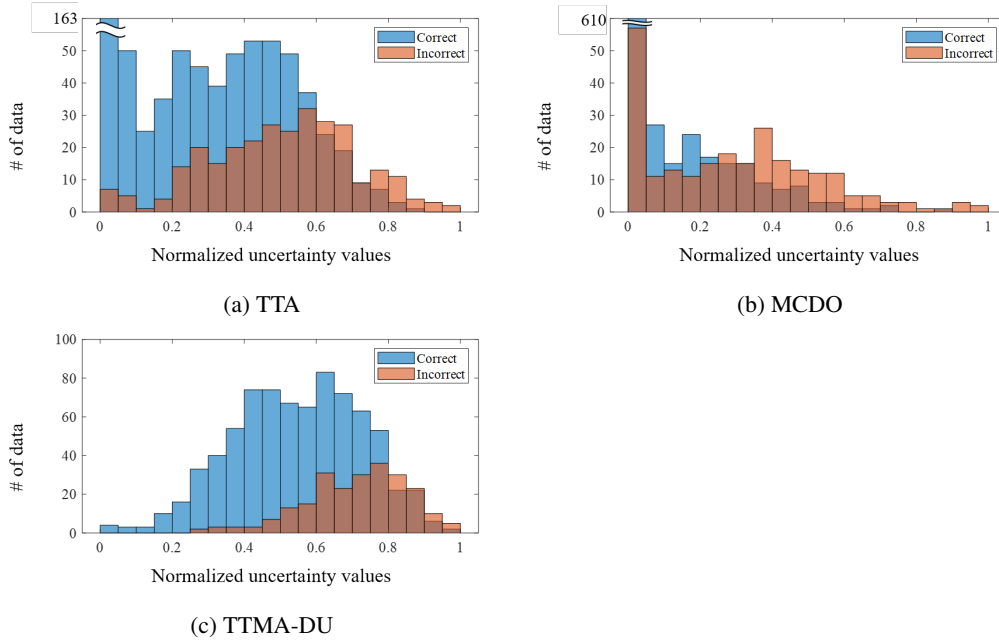


Figure 10: Histograms of aleatoric uncertainty for correct and incorrect test samples for CIFAR-100 classification results with (a) TTA, (b) MCDO, and (c) TTMA-DU methods. In (a) TTA, the number of correct samples having uncertainty of $[0,0.05]$ is 163. In (b) MCDO, the number of correct samples having uncertainty of $[0,0.05]$ is 610.

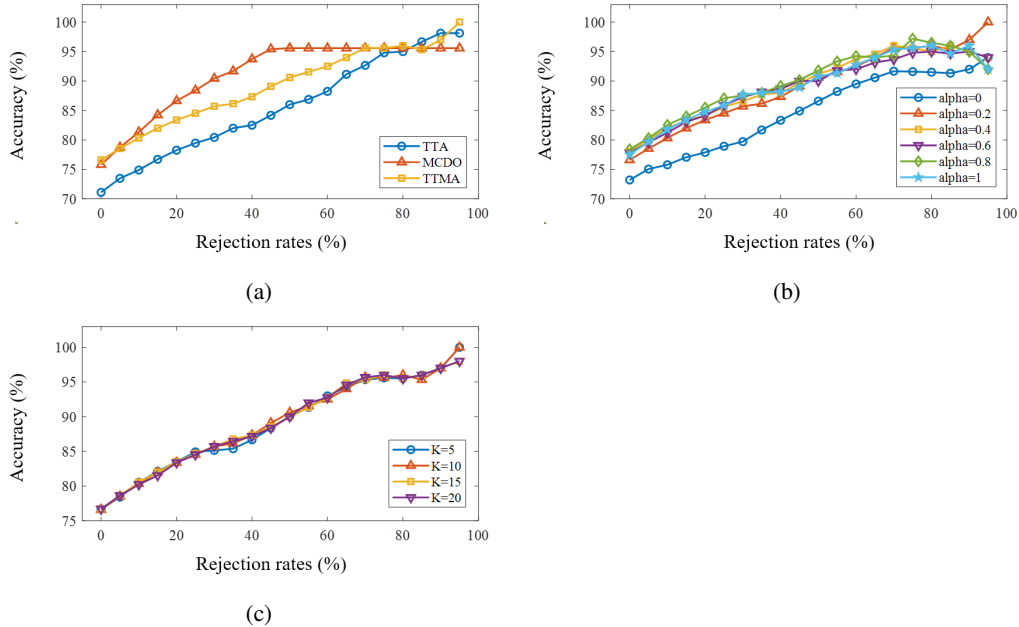


Figure 11: Accuracy-rejection curves of CIFAR-100 classification results with (a) different uncertainty estimation methods, (b) different values of mixup hyper-parameter α , and (c) different values of mixup sampling number K for TTMA-DU.

Fig.13 presents the images of five low TTMA-CDU classes and five high TTMA-CDU classes for five CIFAR-100 test data. It can be observed that the classes with low TTMA-CDU (1) belong to the same super-class, e.g., lion-tiger and baby-boy, or (2) belong to different classes but have similar

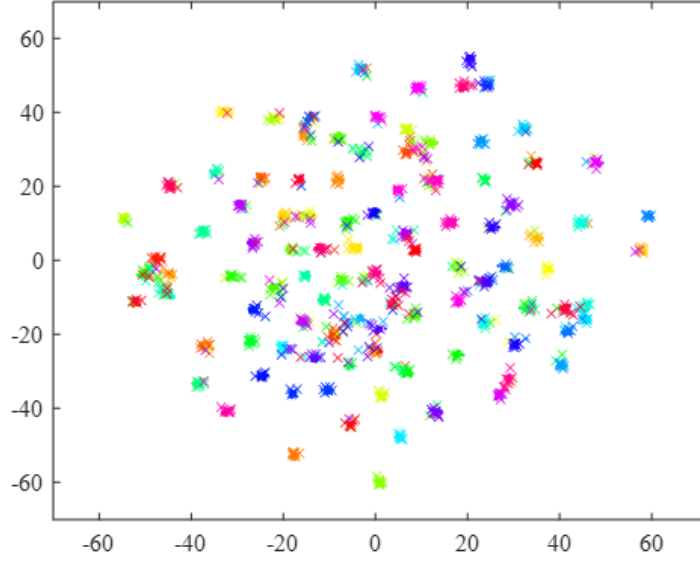


Figure 12: tSNE feature distributions of training (marked as o) and validation (marked as x) data in the CIFAR-100 classification results.

appearances in terms of color and texture, e.g., orange-sunflower, lion-crab, and rose-lobster. In contrast, the high TTMA-CDU classes include classes with different super-classes and appearances, e.g., lion-cup, baby-train, and rose-shark. Fig.14 shows boxplots of (a) TTMA-CDU and (b) AFD for the "orange" class. It can be observed that the low TTMA-CDU classes include (1) classes of the same super-class, e.g., apple and pear, and (2) classes with similar color appearances, e.g., sunflower and chair. On the other hand, the low AFD classes include (1) classes of the same super-class, e.g., apple and pear, and (2) classes of a similar round shape, e.g., sweet pepper, hamster, and bowl. This confirms that the proposed TTMA-CDU provides information on class similarity in a similar manner to AFD for a dataset without class confusion.

Table 3: Performance evaluation and comparisons of CIFAR-100 classification with different uncertainty estimation methods. Accuracy (%) was evaluated on the rejected test data for various rejection rates $T \in \{0\%, 25\%, 50\%, 75\%, 95\%\}$.

Methods	Rejection rates (%)				
	0	25	50	75	95
Single	74.9				
TTA	71.1	79.5	86.0	94.8	98.1
MCDO	75.8	88.4	95.6	95.6	95.6
TTMA-DU ($\alpha = 0.0$)	73.2	78.9	86.6	91.6	94.0
TTMA-DU ($\alpha = 0.2$)	76.6	84.5	90.6	95.6	100
TTMA-DU ($\alpha = 0.4$)	78.0	85.6	91.2	95.6	94.0
TTMA-DU ($\alpha = 0.6$)	77.8	85.9	90.0	94.8	94.0
TTMA-DU ($\alpha = 0.8$)	78.4	87.1	91.8	97.2	92.0
TTMA-DU ($\alpha = 1.0$)	77.5	85.9	90.8	95.6	92.0

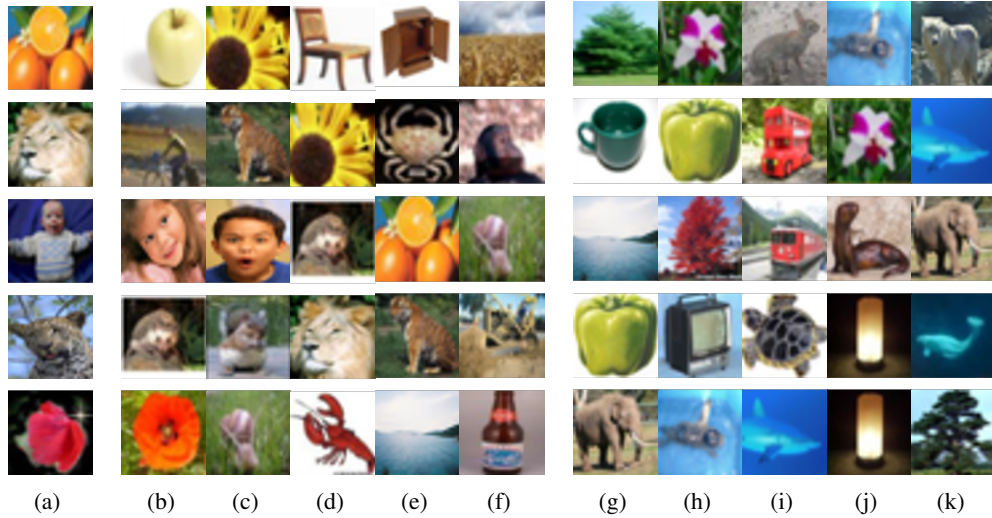
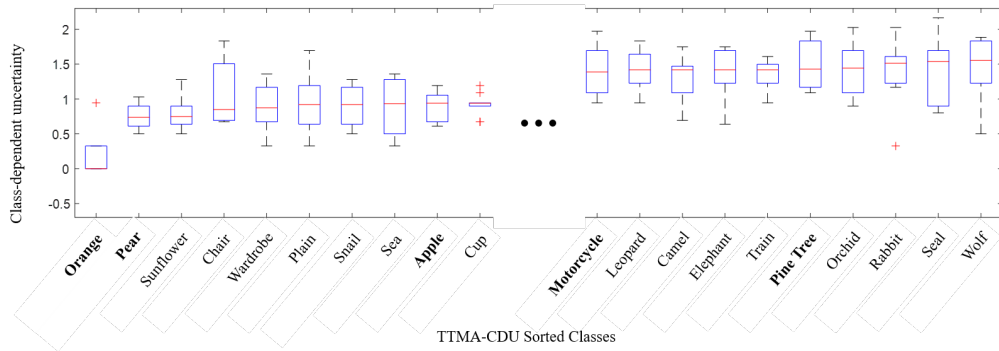
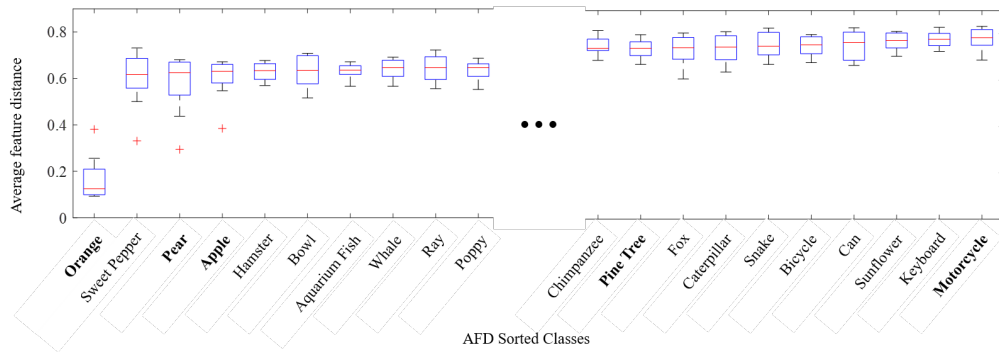


Figure 13: Examples of CIFAR-100 test classes (a) and the classes with the lowest five TTMA-CDU (b-f) and the classes with the highest five TTMA-CDU (g-k). Five example test classes in (a) are orange, lion, baby, leopard, and rose (top to bottom).



(a) TTMA-CDU (Orange)



(b) AFD (Orange)

Figure 14: Boxplots of (a) TTMA class-dependent uncertainty (TTMA-CDU) and (b) average feature distance (AFD) for "orange" class in the CIFAR-100 classification results. Classes are sorted according to the median values. The ten classes with the lowest medians and the ten classes with the highest medians are shown on the left and right sides, respectively. The classes corresponding to both of the lowest/highest ten in-class TTMA-CDU and in-class AFD are shown in bold.

5 DISCUSSION

In this paper, we proposed a method for estimating data and class-dependent uncertainty in image classification using test-time mixup augmentation. Our main contributions can be summarized as follows. First, we introduced a TTMA-DU estimation method and demonstrated its improved performance over existing uncertainty estimation methods in evaluating the reliability of network predictions. Second, we proposed a novel uncertainty measure, TTMA-CDU, which uses the characteristics of mixup augmentation and captures the class confusion and similarity of the trained network. Third, we validated the proposed method on two image classification datasets, and observed consistent results across the different datasets.

To evaluate the reliability of network predictions, one of the key functions of uncertainty estimation is to distinguish between correct and incorrect predictions based on the estimated uncertainty without the need for ground truth. An ideal uncertainty estimation method should assign low uncertainty values to all correct predictions and high uncertainty values to all incorrect predictions. However, CNNs are known to have severe over-confidence characteristics, which results in low uncertainty values for most decisions. To address this, it is necessary to lower the confidence and calibrate the model by applying perturbations to the input data or network or by using ensemble methods for uncertainty estimation. Both TTA and MCDO use perturbations and ensemble techniques, such as affine augmentation of data and dropout on the network, respectively. However, as shown in the experimental results for both datasets, these methods do not fully overcome the low uncertainty issue. This motivated us to consider that a stronger perturbation could lead to a more accurate uncertainty measure. As expected, the proposed TTMA-DU demonstrates improved discrimination between correct and incorrect predictions compared to conventional TTA or MCDO.

To further analyze why the proposed TTMA-DU better distinguished between correct and incorrect predictions than conventional TTA or MCDO, we examine them from the perspective of network ensemble calibration. Table 4 illustrates the expected calibration error (ECE) for the proposed and comparative methods on the ISIC-18 and CIFAR-100 datasets. ECE measures the difference between the predicted confidence and the actual accuracy (Naeini et al., 2015), and a lower ECE indicates a better-calibrated network. As shown in Table 4, the proposed TTMA has higher ECEs than TTA and MCDO. This aligns with recent findings on the relationship between mixup augmentation, ensemble learning, and network calibration (Wen et al., 2021). Wen *et al.* reported that mixup and ensemble have the effect of lowering the confidence of over-confident deep neural networks and when both mixup and ensemble are applied, the effects are accumulated, leading to an under-confident network. This under-confidence characteristic of TTMA can also be observed from the uncertainty distributions in Fig.5 and Fig.10. The proposed TTMA has a smooth confidence distribution relative to those of TTA and MCDO, and the entropy-based uncertainty is also distributed at higher values than those of TTA and MCDO. This under-confidence characteristic of the proposed method improves the distinction between correct and incorrect predictions by further increasing the uncertainty values of incorrect predictions, making it more difficult for the model to be confident in its incorrect predictions. This results in a more reliable and accurate uncertainty measure for distinguishing correct from incorrect predictions.

Table 4: Expected calibration error (ECE) evaluation and comparison of ISIC-18 and CIFAR-100 classification results with different uncertainty estimation methods.

Methods	Datasets	
	ISIC-18	CIFAR-100
Single	0.0729	0.0992
TTA	0.0878	0.1475
MCDO	0.1316	0.1638
TTMA ($\alpha = 0.0$)	0.1686	0.3733
TTMA ($\alpha = 0.2$)	0.2196	0.3641
TTMA ($\alpha = 0.4$)	0.1663	0.3687
TTMA ($\alpha = 0.6$)	0.1529	0.3586
TTMA ($\alpha = 0.8$)	0.0958	0.3538
TTMA ($\alpha = 1.0$)	0.1750	0.3378

In addition, we proposed TTMA-CDU, a novel uncertainty measure that takes into account both data and classes together and evaluated its effectiveness through experiments. While TTMA-DU calculates uncertainty through test-time perturbation using mixup with training data sampled from all classes, TTMA-CDU calculates uncertainty using mixup with training data sampled from a specific class. This can provide information related to prediction instability between the target data and a given class. We hypothesized that TTMA-CDU would provide information related to class confusion and class similarity. In experiments, by comparing the proposed TTMA-CDU with AFD in tSNE feature space, we confirmed that in situations of class confusion, where classes overlap in tSNE feature space, low AFD and high TTMA-CDU were observed. On the other hand, in situations of class similarity, where classes are close but separated each other in tSNE feature space, AFD and TTMA-CDU tend to show similar tendencies. This confirms that the TTMA-CDU not only provides information about class similarity like AFD but also can distinguish class confusion from class similarity through its combination with AFD. Additionally, it is worth noting that TTMA-CDU is able to provide more insights on the model’s understanding of the data, by highlighting classes that are easily confused with one another. This can be useful for further fine-tuning the model, or for identifying areas where additional data or annotation is needed. Overall, the proposed TTMA-CDU method is a promising tool for evaluating and improving the performance of trained network, as it can provide valuable information about the model’s uncertainty and understanding of the data.

6 CONCLUSION

In this paper, we proposed an uncertainty estimation method for deep learning classification using test-time mixup augmentation (TTMA). The main contributions of our method are as follows: (1) the proposed TTMA data uncertainty (TTMA-DU) demonstrated improved reliability in evaluating network predictions compared to existing aleatoric uncertainty methods such as TTA and MCDO due to the aggressive perturbation characteristics of mixup augmentation; (2) we introduced a novel uncertainty measure called the TTMA class-dependent uncertainty (TTMA-CDU), which provides insight into the class confusion and class similarity of the trained network; (3) we performed experiments that showed that both proposed uncertainty measures had the expected performance and behavior on two different image classification datasets. In future work, we plan to improve the performance of TTMA by using mixup variants such as CutMix (Yun et al., 2019) and AugMix (Hendrycks* et al., 2020), and to utilize TTMA uncertainty to increase the accuracy of network predictions.

ACKNOWLEDGMENTS

This work was supported by the National Research Foundation of Korea Grant funded by the Korea government (MSIT) (No. 2020R1A2C1102140), and by the Korea Health Technology R&D Project through the Korea Health Industry Development Institute (KHIDI), funded by the Ministry of Health & Welfare, Republic of Korea (Grant number: HI22C1496)

REFERENCES

- Moloud Abdar, Farhad Pourpanah, Sadiq Hussain, Dana Rezazadegan, Li Liu, Mohammad Ghavamzadeh, Paul Fieguth, Xiaochun Cao, Abbas Khosravi, U. Rajendra Acharya, Vladimir Makarenkov, and Saeid Nahavandi. A review of uncertainty quantification in deep learning: Techniques, applications and challenges. *Information Fusion*, 2021.
- Murat Seçkin Ayhan, Laura Kühlewein, Gulnar Aliyeva, Werner Inhoffen, Focke Ziemssen, and Philipp Berens. Expert-validated estimation of diagnostic uncertainty for deep neural networks in diabetic retinopathy detection. *Medical Image Analysis*, 64:101724, 2020.
- M. Saiful Bari, Muhammad Tasnim Mohiuddin, and Shafiq R. Joty. Multimix: A robust data augmentation strategy for cross-lingual NLP. *CoRR*, abs/2004.13240, 2020.
- Charles Blundell, Julien Cornebise, Koray Kavukcuoglu, and Daan Wierstra. Weight uncertainty in neural networks. In *Proceedings of the 32nd International Conference on International Conference on Machine Learning - Volume 37, ICML’15*, pp. 1613–1622, 2015.

-
- Gustavo Carneiro, Leonardo Zorron Cheng Tao Pu, Rajvinder Singh, and Alastair Burt. Deep learning uncertainty and confidence calibration for the five-class polyp classification from colonoscopy. *Medical Image Analysis*, 62:101653, 2020.
- Krishna Chaitanya, Ertunc Erdil, Neerav Karani, and Ender Konukoglu. Contrastive learning of global and local features for medical image segmentation with limited annotations. In H. Larochelle, M. Ranzato, R. Hadsell, M.F. Balcan, and H. Lin (eds.), *Advances in Neural Information Processing Systems*, volume 33, pp. 12546–12558. Curran Associates, Inc., 2020.
- Jiaao Chen, Zhenghui Wang, Ran Tian, Zichao Yang, and Diyi Yang. Local additivity based data augmentation for semi-supervised NER. In *Proceedings of the 2020 Conference on Empirical Methods in Natural Language Processing (EMNLP)*, pp. 1241–1251, Online, November 2020. Association for Computational Linguistics. doi: 10.18653/v1/2020.emnlp-main.95.
- Pietro Antonio Cicalese, Aryan Mobiny, Zahed Shahmoradi, Xiongfeng Yi, Chandra Mohan, and Hien Van Nguyen. Kidney level lupus nephritis classification using uncertainty guided bayesian convolutional neural networks. *IEEE Journal of Biomedical and Health Informatics*, 25(2):315–324, 2021.
- Noel C. F. Codella, David Gutman, M. Emre Celebi, Brian Helba, Michael A. Marchetti, Stephen W. Dusza, Aadi Kalloo, Konstantinos Liopyris, Nabin K. Mishra, Harald Kittler, and Allan Halpern. Skin lesion analysis toward melanoma detection: A challenge at the 2017 international symposium on biomedical imaging (isbi), hosted by the international skin imaging collaboration (ISIC). *CoRR*, abs/1710.05006, 2017.
- Noel C. F. Codella, David Gutman, M. Emre Celebi, Brian Helba, Michael A. Marchetti, Stephen W. Dusza, Aadi Kalloo, Konstantinos Liopyris, Nabin Mishra, Harald Kittler, and Allan Halpern. Skin lesion analysis toward melanoma detection: A challenge at the 2017 international symposium on biomedical imaging (isbi), hosted by the international skin imaging collaboration (isic). In *2018 IEEE 15th International Symposium on Biomedical Imaging (ISBI 2018)*, pp. 168–172, 2018.
- Noel C. F. Codella, Veronica Rotemberg, Philipp Tschandl, M. Emre Celebi, Stephen W. Dusza, David Gutman, Brian Helba, Aadi Kalloo, Konstantinos Liopyris, Michael A. Marchetti, Harald Kittler, and Allan Halpern. Skin lesion analysis toward melanoma detection 2018: A challenge hosted by the international skin imaging collaboration (ISIC). *CoRR*, abs/1902.03368, 2019.
- Marc Combalia, Noel C. F. Codella, Veronica Rotemberg, Brian Helba, Veronica Vilaplana, Ofer Reiter, Cristina Carrera, Alicia Barreiro, Allan C. Halpern, Susana Puig, and Josep Malveyh. Bcn20000: Dermoscopic lesions in the wild, 2019.
- Steffen Czolbe, Kasra Arnavaz, Oswin Krause, and Aasa Feragen. Is segmentation uncertainty useful? In Aasa Feragen, Stefan Sommer, Julia Schnabel, and Mads Nielsen (eds.), *Information Processing in Medical Imaging*, pp. 715–726, Cham, 2021.
- Ali Dabouei, Sobhan Soleymani, Fariborz Taherkhani, and Nasser M. Nasrabadi. Supermix: Supervising the mixing data augmentation. In *Proceedings of the IEEE/CVF Conference on Computer Vision and Pattern Recognition (CVPR)*, pp. 13794–13803, June 2021.
- Jeffrey De Fauw, Joseph R. Ledsam, Bernardino Romera-Paredes, Stanislav Nikolov, Nenad Tomasev, Sam Blackwell, Harry Askham, Xavier Glorot, Brendan O’Donoghue, Daniel Visentin, George van den Driessche, Balaji Lakshminarayanan, Clemens Meyer, Faith Mackinder, Simon Bouton, Kareem Ayoub, Reena Chopra, Dominic King, Alan Karthikesalingam, Cían O. Hughes, Rosalind Raine, Julian Hughes, Dawn A. Sim, Catherine Egan, Adnan Tufail, Hugh Montgomery, Demis Hassabis, Geraint Rees, Trevor Back, Peng T. Khaw, Mustafa Suleyman, Julien Cornebise, Pearse A. Keane, and Olaf Ronneberger. Clinically applicable deep learning for diagnosis and referral in retinal disease. *Nature Medicine*, 24(9):1342–1350, Sep 2018.
- Zach Eaton-Rosen, Felix Bragman, Sebastien Ourselin, and M Jorge Cardoso. Improving data augmentation for medical image segmentation. 2018.

-
- Geoffrey French, Timo Aila, Samuli Laine, Michal Mackiewicz, and Graham D. Finlayson. Consistency regularization and cutmix for semi-supervised semantic segmentation. *CoRR*, abs/1906.01916, 2019.
- Yarin Gal and Zoubin Ghahramani. Dropout as a bayesian approximation: Representing model uncertainty in deep learning. In Maria Florina Balcan and Kilian Q. Weinberger (eds.), *Proceedings of The 33rd International Conference on Machine Learning*, volume 48 of *Proceedings of Machine Learning Research*, pp. 1050–1059, New York, New York, USA, 20–22 Jun 2016.
- Yarin Gal, Riashat Islam, and Zoubin Ghahramani. Deep bayesian active learning with image data. *CoRR*, abs/1703.02910, 2017.
- Jakob Gawlikowski, Cedric R. Njitecheu Tassi, Mohsin Ali, Jongseok Lee, Matthias Humt, Jianxiang Feng, Anna M. Kruspe, Rudolph Triebel, Peter Jung, Ribana Roscher, Muhammad Shahzad, Wen Yang, Richard Bamler, and Xiao Xiang Zhu. A survey of uncertainty in deep neural networks. *CoRR*, abs/2107.03342, 2021.
- Florin C. Ghesu, Bogdan Georgescu, Awais Mansoor, Youngjin Yoo, Eli Gibson, R.S. Vishwanath, Abishek Balachandran, James M. Balter, Yue Cao, Ramandeep Singh, Subba R. Digumarthy, Mannudeep K. Kalra, Sasa Grbic, and Dorin Comaniciu. Quantifying and leveraging predictive uncertainty for medical image assessment. *Medical Image Analysis*, 68:101855, 2021.
- Golnaz Ghiasi, Yin Cui, Aravind Srinivas, Rui Qian, Tsung-Yi Lin, Ekin D. Cubuk, Quoc V. Le, and Barret Zoph. Simple copy-paste is a strong data augmentation method for instance segmentation. In *Proceedings of the IEEE/CVF Conference on Computer Vision and Pattern Recognition (CVPR)*, pp. 2918–2928, June 2021.
- Simon Graham, Hao Chen, Jevgenij Gamper, Qi Dou, Pheng-Ann Heng, David Snead, Yee Wah Tsang, and Nasir Rajpoot. Mild-net: Minimal information loss dilated network for gland instance segmentation in colon histology images. *Medical Image Analysis*, 52:199–211, 2019.
- Hongyu Guo, Yongyi Mao, and Richong Zhang. Augmenting data with mixup for sentence classification: An empirical study. *CoRR*, abs/1905.08941, 2019.
- Dan Hendrycks*, Norman Mu*, Ekin Dogus Cubuk, Barret Zoph, Justin Gilmer, and Balaji Lakshminarayanan. Augmix: A simple method to improve robustness and uncertainty under data shift. In *International Conference on Learning Representations*, 2020.
- Lisa Herzog, Elvis Murina, Oliver Dürr, Susanne Wegener, and Beate Sick. Integrating uncertainty in deep neural networks for mri based stroke analysis. *Medical Image Analysis*, 65:101790, 2020.
- Carl-Johan Hoel, Tommy Tram, and Jonas Sjöberg. Reinforcement learning with uncertainty estimation for tactical decision-making in intersections. *CoRR*, abs/2006.09786, 2020a.
- Carl-Johan Hoel, Krister Wolff, and Leo Laine. Tactical decision-making in autonomous driving by reinforcement learning with uncertainty estimation. *CoRR*, abs/2004.10439, 2020b.
- SeulGi Hong, Heonjin Ha, Junmo Kim, and Min-Kook Choi. Deep active learning with augmentation-based consistency estimation. *CoRR*, abs/2011.02666, 2020.
- Wonmo Jung, Sejin Park, Kyu-Hwan Jung, and Sung Il Hwang. Prostate cancer segmentation using manifold mixup u-net. In *International Conference on Medical Imaging with Deep Learning—Extended Abstract Track*, 2019.
- Kumara Kahatapitiya, Zhou Ren, Haoxiang Li, Zhenyu Wu, and Michael S. Ryoo. Self-supervised pretraining with classification labels for temporal activity detection. *CoRR*, abs/2111.13675, 2021.
- Alex Kendall and Yarin Gal. What uncertainties do we need in bayesian deep learning for computer vision? In I. Guyon, U. V. Luxburg, S. Bengio, H. Wallach, R. Fergus, S. Vishwanathan, and R. Garnett (eds.), *Advances in Neural Information Processing Systems*, volume 30, 2017.

-
- Jang-Hyun Kim, Wonho Choo, and Hyun Oh Song. Puzzle mix: Exploiting saliency and local statistics for optimal mixup. In Hal Daumé III and Aarti Singh (eds.), *Proceedings of the 37th International Conference on Machine Learning*, volume 119 of *Proceedings of Machine Learning Research*, pp. 5275–5285, 13–18 Jul 2020a.
- Jongmok Kim, Jooyoung Jang, and Hyunwoo Park. Structured consistency loss for semi-supervised semantic segmentation. *CoRR*, abs/2001.04647, 2020b.
- Taeoh Kim, Hyeongmin Lee, MyeongAh Cho, Ho Seong Lee, Dong Heon Cho, and Sangyoung Lee. Learning temporally invariant and localizable features via data augmentation for video recognition. *CoRR*, abs/2008.05721, 2020c.
- Balaji Lakshminarayanan, Alexander Pritzel, and Charles Blundell. Simple and scalable predictive uncertainty estimation using deep ensembles. In *Proceedings of the 31st International Conference on Neural Information Processing Systems, NIPS’17*, pp. 6405–6416, 2017.
- Yanghao Li, Chao-Yuan Wu, Haoqi Fan, Karttikeya Mangalam, Bo Xiong, Jitendra Malik, and Christoph Feichtenhofer. Improved multiscale vision transformers for classification and detection. *CoRR*, abs/2112.01526, 2021.
- Zeju Li, Konstantinos Kamnitsas, and Ben Glocker. Overfitting of neural nets under class imbalance: Analysis and improvements for segmentation. In *International Conference on Medical Image Computing and Computer-Assisted Intervention*, pp. 402–410. Springer, 2019.
- Zicheng Liu, Siyuan Li, Di Wu, Zhiyuan Chen, Lirong Wu, Jianzhu Guo, and Stan Z. Li. Automix: Unveiling the power of mixup. *CoRR*, abs/2103.13027, 2021.
- Rémi Martin, Joaquim Miró, and Luc Duong. Epistemic uncertainty modeling for vessel segmentation. In *2019 41st Annual International Conference of the IEEE Engineering in Medicine and Biology Society (EMBC)*, pp. 5923–5927, 2019.
- Kazuhisa Matsunaga, Akira Hamada, Akane Minagawa, and Hiroshi Koga. Image classification of melanoma, nevus and seborrheic keratosis by deep neural network ensemble. *CoRR*, abs/1703.03108, 2017.
- Jishnu Mukhoti, Andreas Kirsch, Joost van Amersfoort, Philip H. S. Torr, and Yarin Gal. Deterministic neural networks with appropriate inductive biases capture epistemic and aleatoric uncertainty. *CoRR*, abs/2102.11582, 2021.
- Mahdi Pakdaman Naeini, Gregory F. Cooper, and Milos Hauskrecht. Obtaining well calibrated probabilities using bayesian binning. In *Proceedings of the Twenty-Ninth AAAI Conference on Artificial Intelligence, AAAI’15*, pp. 2901–2907. AAAI Press, 2015. ISBN 0262511290.
- Christopher Nielsen and Michal Okoniewski. Gan data augmentation through active learning inspired sample acquisition. In *Proceedings of the IEEE/CVF Conference on Computer Vision and Pattern Recognition (CVPR) Workshops*, June 2019.
- Egor Panfilov, Aleksei Tiulpin, Stefan Klein, Miika T Nieminen, and Simo Saarakkala. Improving robustness of deep learning based knee mri segmentation: Mixup and adversarial domain adaptation. In *Proceedings of the IEEE/CVF International Conference on Computer Vision Workshops*, pp. 0–0, 2019.
- Jie Qin, Jiemin Fang, Qian Zhang, Wenyu Liu, Xingang Wang, and Xinggang Wang. Resizemix: Mixing data with preserved object information and true labels, 2020.
- Jonathan G. Richens, Ciarán M. Lee, and Saurabh Johri. Improving the accuracy of medical diagnosis with causal machine learning. *Nature Communications*, 11(1):3923, Aug 2020.
- Mamshad Nayeem Rizve, Kevin Duarte, Yogesh S Rawat, and Mubarak Shah. In defense of pseudo-labeling: An uncertainty-aware pseudo-label selection framework for semi-supervised learning. In *International Conference on Learning Representations*, 2021.

-
- Afshar Shamsi, Hamzeh Asgharnezhad, Shirin Shamsi Jokandan, Abbas Khosravi, Parham M. Ke-bria, Darius Nahavandi, Saeid Nahavandi, and Dipti Srinivasan. An uncertainty-aware transfer learning-based framework for covid-19 diagnosis. *IEEE Transactions on Neural Networks and Learning Systems*, 32(4):1408–1417, 2021.
- Chenglei Si, Zhengyan Zhang, Fanchao Qi, Zhiyuan Liu, Yasheng Wang, Qun Liu, and Maosong Sun. Better robustness by more coverage: Adversarial training with mixup augmentation for robust fine-tuning. *CoRR*, abs/2012.15699, 2020.
- Karen Simonyan and Andrew Zisserman. Very deep convolutional networks for large-scale image recognition. In *3rd International Conference on Learning Representations, ICLR 2015*, 2015.
- Rajeev Kumar Singh, Rohan Gorantla, Sai Giridhar Allada, and Narra Pratap. Skinet: A deep learning solution for skin lesion diagnosis with uncertainty estimation and explainability. *CoRR*, abs/2012.15049, 2020.
- Yukun Su, Ruizhou Sun, Guosheng Lin, and Qingyao Wu. Context decoupling augmentation for weakly supervised semantic segmentation. In *Proceedings of the IEEE/CVF International Conference on Computer Vision (ICCV)*, pp. 7004–7014, October 2021.
- Lichao Sun, Congying Xia, Wenpeng Yin, Tingting Liang, Philip Yu, and Lifang He. Mixup-transformer: Dynamic data augmentation for NLP tasks. In *Proceedings of the 28th International Conference on Computational Linguistics*, pp. 3436–3440, Barcelona, Spain (Online), December 2020. International Committee on Computational Linguistics. doi: 10.18653/v1/2020.coling-main.305.
- Xiaolin Tang, Kai Yang, Hong Wang, Jiahang Wu, Yechen Qin, Wenhao Yu, and Dongpu Cao. Prediction-uncertainty-aware decision-making for autonomous vehicles. *IEEE Transactions on Intelligent Vehicles*, 7(4):849–862, 2022.
- Sunil Thulasidasan, Gopinath Chennupati, Jeff A Bilmes, Tanmoy Bhattacharya, and Sarah Michalak. On mixup training: Improved calibration and predictive uncertainty for deep neural networks. In H. Wallach, H. Larochelle, A. Beygelzimer, F. d'Alché-Buc, E. Fox, and R. Garnett (eds.), *Advances in Neural Information Processing Systems*, volume 32, 2019.
- Philipp Tschandl, Cliff Rosendahl, and Harald Kittler. The ham10000 dataset, a large collection of multi-source dermatoscopic images of common pigmented skin lesions. *Scientific Data*, 5(1): 180161, Aug 2018.
- A F M Shahab Uddin, Mst. Sirazam Monira, Wheemyung Shin, TaeChoong Chung, and Sung-Ho Bae. Saliencymix: A saliency guided data augmentation strategy for better regularization. In *International Conference on Learning Representations*, 2021.
- Laurens van der Maaten and Geoffrey Hinton. Visualizing data using t-sne. *Journal of Machine Learning Research*, 9(86):2579–2605, 2008.
- Vikas Verma, Alex Lamb, Christopher Beckham, Amir Najafi, Ioannis Mitliagkas, David Lopez-Paz, and Yoshua Bengio. Manifold mixup: Better representations by interpolating hidden states. In *International Conference on Machine Learning*, pp. 6438–6447. PMLR, 2019.
- Chi-Shiang Wang, Fang-Yi Su, Tsung-Lu Michael Lee, Yi-Shan Tsai, and Jung-Hsien Chiang. Cuab: Convolutional uncertainty attention block enhanced the chest x-ray image analysis, 2021.
- Guotai Wang, Wenqi Li, Michael Aertsen, Jan Deprest, Sébastien Ourselin, and Tom Vercauteren. Aleatoric uncertainty estimation with test-time augmentation for medical image segmentation with convolutional neural networks. *Neurocomputing*, 338:34–45, 2019.
- Yeming Wen, Ghassen Jerfel, Rafael Muller, Michael W Dusenberry, Jasper Snoek, Balaji Lakshminarayanan, and Dustin Tran. Combining ensembles and data augmentation can harm your calibration. In *International Conference on Learning Representations*, 2021.
- Sangdoon Yun, Dongyoon Han, Seong Joon Oh, Sanghyuk Chun, Junsuk Choe, and Youngjoon Yoo. Cutmix: Regularization strategy to train strong classifiers with localizable features. In *Proceedings of the IEEE/CVF International Conference on Computer Vision (ICCV)*, October 2019.

-
- Sangdoon Yun, Seong Joon Oh, Byeongho Heo, Dongyoon Han, and Jinhyung Kim. Videomix: Rethinking data augmentation for video classification. *arXiv preprint arXiv:2012.03457*, 2020.
- Sergey Zagoruyko and Nikos Komodakis. Wide residual networks. In *Proceedings of the British Machine Vision Conference (BMVC)*, pp. 87.1–87.12, September 2016.
- Hongyi Zhang, Moustapha Cisse, Yann N. Dauphin, and David Lopez-Paz. mixup: Beyond empirical risk minimization. In *International Conference on Learning Representations*, 2018.
- Jianpeng Zhang, Yutong Xie, Yong Xia, and Chunhua Shen. Attention residual learning for skin lesion classification. *IEEE Transactions on Medical Imaging*, 38(9):2092–2103, 2019.
- Linjun Zhang, Zhun Deng, Kenji Kawaguchi, and James Zou. When and how mixup improves calibration. *CoRR*, abs/2102.06289, 2021.
- Guang Zhao, Edward Dougherty, Byung-Jun Yoon, Francis Alexander, and Xiaoning Qian. Uncertainty-aware active learning for optimal bayesian classifier. In *International Conference on Learning Representations*, 2021.
- Wei Zhao, Jiancheng Yang, Bingbing Ni, Dexi Bi, Yingli Sun, Mengdi Xu, Xiaoxia Zhu, Cheng Li, Liang Jin, Pan Gao, et al. Toward automatic prediction of egfr mutation status in pulmonary adenocarcinoma with 3d deep learning. *Cancer medicine*, 8(7):3532–3543, 2019.
- Tianfei Zhou, Meijie Zhang, Fang Zhao, and Jianwu Li. Regional semantic contrast and aggregation for weakly supervised semantic segmentation. In *Proceedings of the IEEE/CVF Conference on Computer Vision and Pattern Recognition (CVPR)*, pp. 4299–4309, June 2022.